



# Introduction of a new simple dynamic phantom for physical BOLD effect simulation

Themistoklis Boursianis<sup>1</sup> · Georgios Kalaitzakis<sup>1</sup> · Georgios Gourzoulidis<sup>2,3</sup> · Apostolos Karantanas<sup>4,5</sup> · Efrosini Papadaki<sup>4,5</sup> · Thomas G. Maris<sup>1,5</sup>

Received: 24 June 2021 / Revised: 5 October 2021 / Accepted: 7 October 2021 / Published online: 18 October 2021  
© European Society for Magnetic Resonance in Medicine and Biology (ESMRMB) 2021

## Abstract

**Objective** To propose a new method of simulating the BOLD contrast using a dynamic, easy to construct and operate, low-cost physical phantom.

**Materials and methods** A structure of thin pipelines passing through a gel volume was used to simulate blood vessels in human tissue. Quantitative  $T2^*$ ,  $R2^*$  measurements were used to study the signal change of the phantom. BOLD fMRI experiments and analysis were performed to evaluate its potential use as an fMRI simulator.

**Results** Experimental  $T2^*$ ,  $R2^*$  measurements showed similar behavior with published references. BOLD contrast was successfully achieved with the proposed method. In addition, there were several proposed parameters, like the angle of the phantom relative to  $B_0$ , which can easily adjust the signal change and the activation area. Coefficients of variation showed good reproducibility within a month period. Statistical  $t$  maps were produced with in-house software for the BOLD measurements.

**Discussion**  $T2^*$ -maps and BOLD images confirm the potential use of this phantom as an fMRI simulator and also as a tool for studying sensitivity and specificity of BOLD sequences/algorithms.

**Keywords** fMRI · Phantom · Agarose · BOLD · Simulation

## Introduction

Functional magnetic resonance imaging (fMRI) is an indirect brain activity measuring technique [1, 2]. The most common fMRI method used is Blood Oxygen Level Dependent (BOLD) imaging, which depicts the activated brain regions during a stimulus or a condition. BOLD contrast is defined as the signal difference between baseline and activation states, in  $T2^*$ -weighted ( $T2^*W$ ) MR imaging and it is

generally implemented utilizing fast Gradient Echo–Echo Planar Imaging (GRE EPI) sequences.

During activation, blood flow increases at the stimulated regions of the brain, leading to increased concentration of oxygenated red blood cells in this area. Oxygenated blood cells are diamagnetic, due to the presence of oxy-hemoglobin, in contrast to deoxygenated red blood cells which are paramagnetic, due to the presence of deoxy-hemoglobin [3]. The consequent magnetic susceptibility difference creates

✉ Themistoklis Boursianis  
tboursianis@gmail.com

Georgios Kalaitzakis  
giorgo.kalaitzakis@gmail.com

Georgios Gourzoulidis  
gourz@yahoo.com

Apostolos Karantanas  
akarantanas@gmail.com

Efrosini Papadaki  
fpapada@otenet.gr

Thomas G. Maris  
tmaris@med.uoc.gr

<sup>1</sup> Department of Medical Physics, University of Crete, Heraklion, Crete, Greece

<sup>2</sup> Research and Measurements Center of OHS Hazardous Agents, OHS Directorate, Hellenic Ministry of Labor, Athens, Greece

<sup>3</sup> Lighting Lab, National Technical University of Athens, Athens, Greece

<sup>4</sup> Department of Radiology, University of Crete, Heraklion, Crete, Greece

<sup>5</sup> Computational BioMedicine Laboratory, Institute of Computer Science, Foundation for Research and Technology-Hellas (FORTH), Heraklion, Crete, Greece

a small signal increase in the active area, just a 1–3% (at 1.5 T) difference compared to the actual (baseline) signal. Sophisticated image post-processing and statistical methods are applied to extract this slight signal difference [4].

The final result is a superimposed anatomical image, usually a 3D T1-weighted (*w*) image which exhibits high grey to white matter contrast. The color map/spots are related to the statistical significance of changes for a particular condition/activation as compared to a baseline condition without any activation state, or stimulus [5].

GRE EPI sequences provide the sensitivity required for the BOLD effect, due to their inherent T2\* weighting and fast data acquisition. Typical acquisition time of BOLD EPI for the whole brain volume falls within the range of 2–3 s; the image quality though, is downgraded from noise and artifacts that may consequently affect the BOLD results.

Concerning the quality assurance (QA) of the fMRI protocols, static phantoms filled with water or gels have been used to measure parameters such as signal-to-noise (SNR), contrast-to-noise (CNR) or ghosting ratios (GR) [6]. Static phantoms, though, are not able to provide dynamic signal change which could simulate the basic BOLD effect. Few studies in the literature have proposed the use of dynamic physical phantoms in a QA procedure, in order to optimize not only all the parameters that affect the image quality, but also the BOLD signal sensitivity and specificity.

Olsrud et al. [7] introduced a two-compartment gel phantom that produces the BOLD effect by manually alternating two imaging volumes with different T2\*. It produces a homogenous signal enhancement in a relatively large volume, which in turn can provide adequate activation area (a circle of 44 mm diameter) in the obtained images. However, that approach has limited adjustment properties, since the signal enhancement is limited into the signal difference of the two gels used.

Moreover, SmartPhantom [8] generates a signal change utilizing a quadrature architecture radio frequency transmit coil, which can be externally activated by comprising two perpendicular planar loops. In this approach, the signal enhancement is adjustable by changing the enhancement loop circuit, but the origin of this signal enhancement differs from real BOLD and can be dependent on the position of the phantom in the receiver coil or on different coils.

In another study, electric current is applied to a thin wire within a proton-rich medium, to induce a distortion of the magnetic field that can regenerate BOLD contrast [9, 10]. These phantoms, produce an adjustable but inhomogeneous activation area near the wire (several pixels). Also, many false activated pixels appear in the obtained images for analysis.

All the above-mentioned dynamic phantoms do provide the necessary BOLD measurements signal change. This signal change is, however, indirectly produced, without truly

simulating the physical basis of the BOLD effect. The latter considers that the susceptibility difference produces the T2\* signal change in the active and the non-active states, respectively. Furthermore, the dynamic phantoms that implement electrical signal require an electronic circuit, making them rather complex to manufacture and operate.

In the current study, a new method for the BOLD effect simulation is presented, using a simple, easy to construct and operate, low-cost dynamic phantom. The rationale of the proposed method is based upon the simulation of blood vessels in human tissues with a simple structure of small pipelines passing through a specific gel volume. Different mediums were injected in the pipelines to induce a local change in magnetic susceptibility, without contributing to the MR signal acquired. The potential use of the proposed method to recreate BOLD contrast was evaluated using T2\* maps. Moreover, a BOLD experiment was performed and a preliminary implementation of the phantom in TE optimization process is presented.

## Materials and methods

### Phantom fabrication

#### Structure

An acrylic (PMMA) parallelepiped container of internal dimensions  $10 \times 10 \times 12 \text{ cm}^3$  and wall thickness of 1 cm was constructed to be filled with agarose gel. A thin plastic pipe runs through holes on the two opposed planes of the container and through its entire volume. The plastic pipe's inner diameter was 0.5 mm and its outer diameter 0.85 mm, imitating a draining venous vessel in human tissue. The phantom structure and a photo of an empty phantom are presented (Fig. 1).

The rationale behind the above construction is that the phantom has to be filled with an MRI visible material, to be scanned having the small pipe either empty (full of air) or filled with any low viscosity liquid that can easily flow through it utilizing a simple clinical syringe. The presence of this liquid and, also, the pipe material itself induce a local distortion of the magnetic field homogeneity, according to their magnetic susceptibility properties, that alters the measured signal from the surrounding material. The whole pipe volume is a small fraction ( $\sim 1/15$ ) of the imaging voxel volume (Fig. 2) of the BOLD sequence (usually  $3 \times 3 \times 3 \text{ mm}^3$ ).

#### Agarose gel

Agarose gel was selected as the MRI visible material. The T2\* of the human gray matter at 1.5 T lies in the range of 60–80 ms as measured in a recent study [11]. To the best

**Fig. 1** The phantom structure (a). Photo of the empty phantom (b)

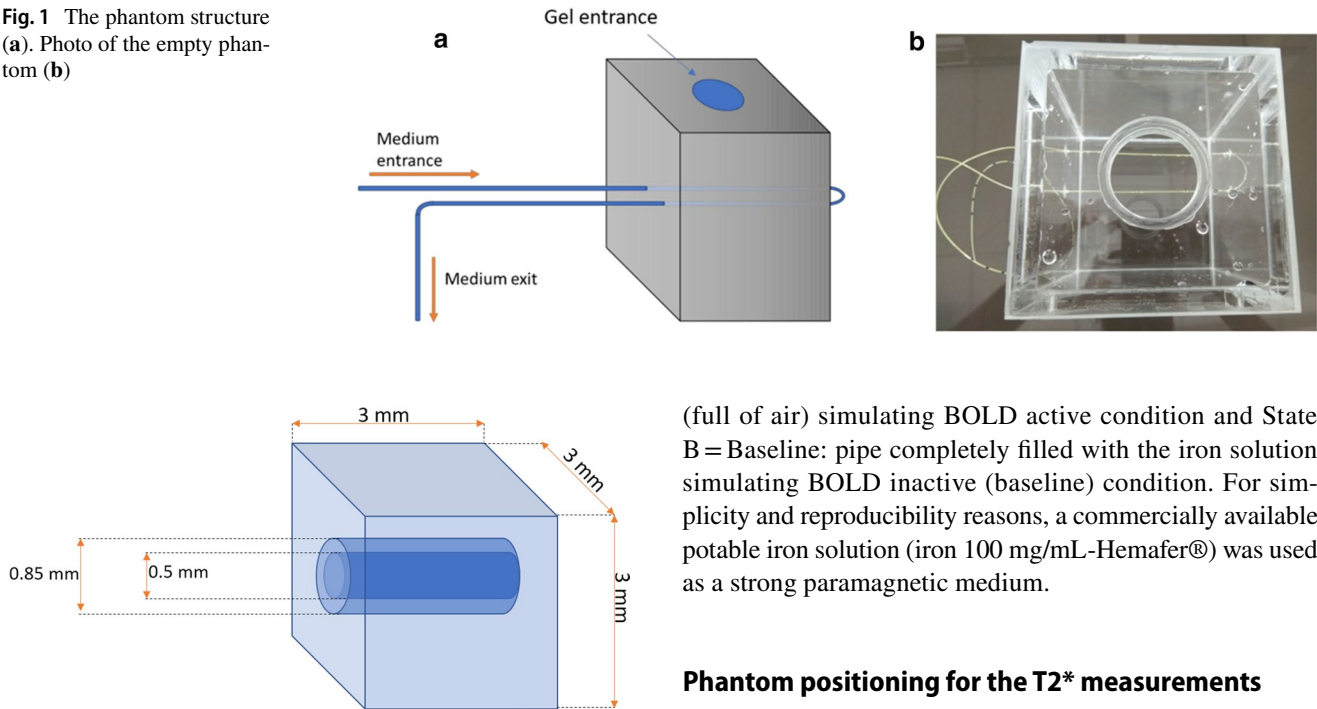


**Fig. 2** The pipe structure inside the imaging voxel

of our knowledge, there are no studies examining the agarose gel  $T_2^*$  dependence with respect to the concentration. Therefore, this selection was based on the dependence of  $T_2$  relaxation time on the agarose concentration (even though the relevant  $T_1$  and  $T_2$  values dependence was not taken under consideration in this study). According to [12, 13],  $T_2$  value of 2% agarose gel is in the range of 60–70 ms. Thus, the  $T_2^*$  is expected to be slightly lower, depending on the field strength and homogeneity. Based on the above and trying to keep the procedure simple, the phantom was filled with 2% (w/v) agarose gel.

### Media to be injected

Various materials were tested to decide on the best combination for the BOLD simulation. When water was injected in the pipes, the signal of the voxel increased not only by its susceptibility effects to its neighborhood, but also by its own contribution to the signal of the specific voxel. Water provides a strong signal in the  $T_2^*$ W images due to its long  $T_2/T_2^*$ . Even though the volume of the pipe's medium is a very small fraction of the voxel volume (Fig. 2), its signal was greatly increased. Trying to eliminate the signal contribution of the medium in the pipe, air and a strong paramagnetic iron solution were chosen as the mediums to be injected sequentially in the pipe, generating the two states of the phantom to simulate the two conditions (active/baseline) of BOLD experiments. In other words, State A = Active: empty pipe

(full of air) simulating BOLD active condition and State B = Baseline: pipe completely filled with the iron solution simulating BOLD inactive (baseline) condition. For simplicity and reproducibility reasons, a commercially available potable iron solution (iron 100 mg/mL-Hemafer®) was used as a strong paramagnetic medium.

### Phantom positioning for the $T_2^*$ measurements

The absolute induced susceptibility or the susceptibility difference between the two mediums selected is not crucial because it can be easily adjusted by another parameter. The pipe's orientation with respect to the  $B_0$  magnetic flux orientation is an important aspect of the phantom, as it has been shown that the magnetic field distribution in the presence of an anisotropic structure like a cylinder depends on the orientation of its long axis with respect to  $B_0$ . Yablonskiy et al. [14, 15] analytically calculated and experimentally measured the signal decay of a medium consisted of parallel cylinders. The  $R_2^*$  measurements in a medium of parallel cylinders have an angular dependence that can be approximated to  $\sin^2\theta$  (or  $-\cos 2\theta$ ), where  $\theta$  is the orientation angle between the long axis of the cylinders and  $B_0$  [16–18].

To measure the angle  $\theta$  dependence of the magnetic field susceptibility induced, the following procedure was implemented. The phantom was positioned in such way that the pipes were parallel to the coronal plane of the scanner during all acquisitions and angle  $\theta$  was adjusted by rotating the whole phantom for different angles with respect to  $B_0$ , remaining on the coronal plane. For each position, a  $T_2^*$  map was obtained, to study the spatial signal change in the pipe region. Five different positions were tested (Fig. 3), for different angles  $\theta$  between the pipe and the  $B_0$  magnetic field lines (approximately  $0^\circ$ ,  $30^\circ$ ,  $45^\circ$ ,  $60^\circ$ ,  $90^\circ$ ). For each position the phantom was scanned for state A and B sequentially. Concerning reproduction, each position was marked on the head coil base. The image orientation (Field Of View) was the same for all phantom positions, to measure the exact angle  $\theta$ . That was precisely measured with the angle measuring tool of image J software on the obtained images. The ten

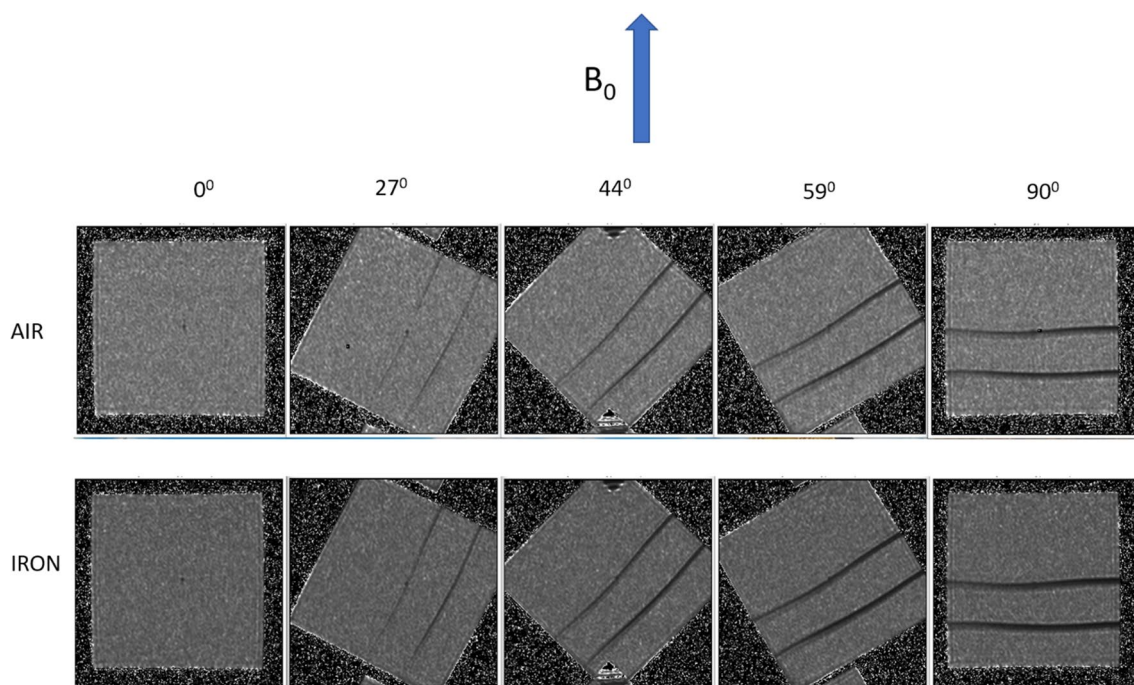


**Fig. 3** Coronal T2\* parametric maps of the same orientation at five different positions. Both phantom conditions (air filled or iron filled pipe) are presented. The measured angle  $\theta$  between  $B_0$  and the pipes is shown

images (T2\* maps) with the different positions are presented (Fig. 3).

### MR image acquisition for the T2\* measurements

A whole-body clinical MRI system 1.5 T (MAGNETOM Sonata/Vision Hybrid, Siemens Healthcare, Erlangen, Germany), equipped with a powerful gradient system (Gradient maximum strength: 40 mT/m, Gradient rise time: 200  $\mu$ s, Gradient Slew rate: 200 mT/m/ms) was utilized. A standard quadrature RF bird cage body coil was used for signal excitation and a two-channel, two-loops, circular polarization head coil (from the same vendor) was used for signal detection.

The phantom was scanned for all five different angles  $\theta$  and for both states A and B with a clinical 2D multi-slice-multi-TE (12 echoes) Gradient Echo Fast Low Angle Shot (FLASH) sequence. The sequence parameters are shown in Table 1.

### Post-processing the T2\* images

All signals were weighted prior to their fitting, to the standard linear fit on all logarithmic TE value signal intensities of the T2\* decay data as described in the literature [19, 20],[21]. T2\* maps were produced for each different position and for each different condition (state A or B) (Fig. 3) on a separate workstation utilizing an in-house software (QMRI

**Table 1** The basic parameters of the MR sequences

| Parameters                       | 2D multi GRE-FLASH  | FID-GRE EPI (BOLD)                             |
|----------------------------------|---|--|
| Field of view (mm <sup>2</sup> ) | 120×120   | 192×192  |
| Acquisition matrix               | 128×128, interpolated to 256×256  | 64×64  |
| Slice orientation                | Coronal, no interslice gap  | Coronal, no interslice gap                     |
| Slice thickness (mm)             | 3   | 3  |
| Flip angle (°)                   | 25  | 90   |
| Pixel bandwidth (Hz/Pixel)       | 450   | 3255   |
| Repetition time (ms)             | 1300  | 4270   |
| Echo time (ms)                   | 2.4, 4.8, 7.21, 9.62, 12.03, 14.44, 16.85, 19.26, 21.67, 24.08, 26.49, 26.9 | 25, 30, 35, 40, 45, 50, 55, 60, 65, 70, 75, 80 |
| Number of slices                 | 32  | 36   |

utilities—X), implemented on a Java platform (64-bit JDK 6u45) designed for this purpose by two of the authors (GK, TGM).

Using ImageJ software and the angle measuring tool, a precise measurement of the angle  $\theta$  was performed. In this sense, the five positions (approximately  $0^\circ$ ,  $30^\circ$ ,  $45^\circ$ ,  $60^\circ$ ,  $90^\circ$ ) were measured ( $0^\circ$ ,  $27^\circ$ ,  $44^\circ$ ,  $59^\circ$ ,  $90^\circ$ ), respectively.

When the pipes are in parallel with  $B_0$  ( $\theta = 0^\circ$ ), no signal drop is observed in both states (Fig. 3). Increasing the angle  $\theta$ , a signal drop appears at the pipes' region. The state's B (iron filled pipe) signal drop seems to be higher than the state's A signal drop (air filled pipe) for all angles.

To quantify this signal drop, the  $T_2^*$  values were measured across the perpendicular axis of the pipes, using a thick profile (10 pixels) line of 50 mm length (Fig. 4). The profile across the presented  $T_2^*$  map ( $\theta = 44^\circ$ ) indicates a background value of 62 ms and a significant drop at the pipe's region pixels (Fig. 4). The width and the intensity of the response indicate the strength of the susceptibility effect of the pipe on the  $T_2^*$  measured value. The basal width

(width at 62 ms) of the two low  $T_2^*$  lobes and the lowest  $T_2^*$  value of the lobes for each angle and each state is shown in Table 2.

The relevant  $R_2^*$  maps ( $R_2^* = 1/T_2^*$  in  $\text{sec}^{-1}$  units) were also constructed utilizing the in-house software (QMRI utilities—X). As above, similar  $R_2^*$  profiles were used to measure the peak  $R_2^*$  value on the pipes' region on the  $R_2^*$  maps. These  $R_2^*$  peak values were plotted against the angle  $\theta$  and  $\sin^2\theta$  (Fig. 5).

**BOLD experiment**

**Operation, position, and image acquisition**

BOLD experiment requires a switch between two states: Baseline and Active. The switching between the active and the baseline state was performed by manually injecting in the pipe either the iron solution, or air with two syringes. The injection time was less than a second since the whole pipe's volume for its entire 1-m length was about 0.2 ml. The

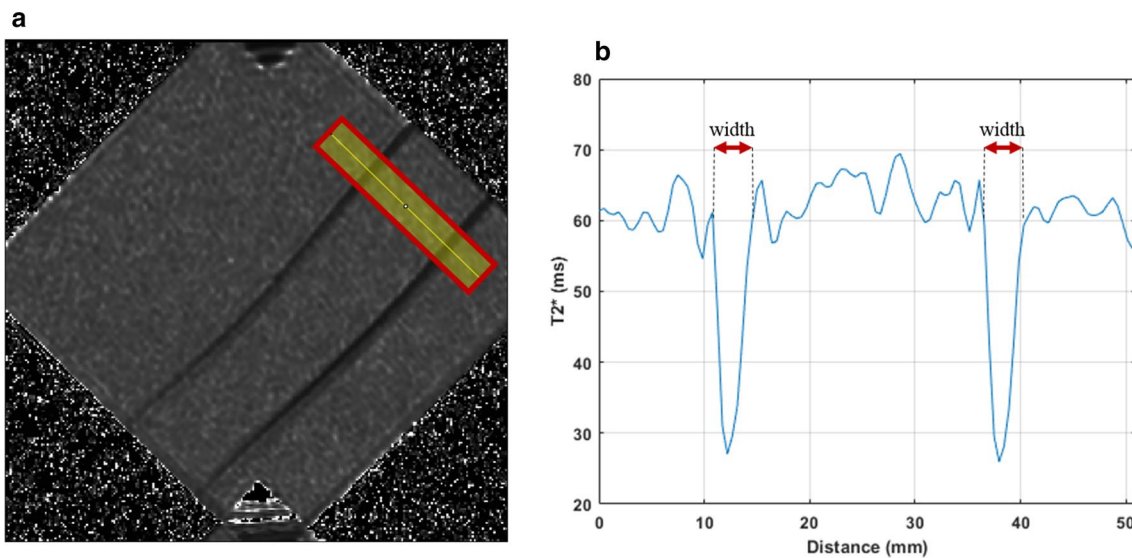


**Fig. 4**  $T_2^*$  (ms) parametric map at  $\theta = 44^\circ$ , B state (a). The corresponding profile across the perpendicular axis to the pipes' direction (b)

**Table 2** The lowest peak value (ms) of the thick  $T_2^*$  profile (Fig. 3) for each different angle and for each different state

| State | Angle ( $^\circ$ ) | 0     |         | 27         |         | 44    |         | 59    |         | 90    |         |
|-------|--------------------|-------|---------|------------|---------|-------|---------|-------|---------|-------|---------|
|       |                    | Width | $T_2^*$ | Width      | $T_2^*$ | Width | $T_2^*$ | Width | $T_2^*$ | Width | $T_2^*$ |
| A     | Pipe 1             | 0     | 62      | 2.1        | 49.2    | 3.1   | 30      | 3.7   | 23.5    | 5.2   | 18.3    |
|       | Pipe 2             | 0     | 62      | 2.4        | 50.3    | 3.4   | 30.5    | 3.5   | 22.5    | 5.2   | 18.1    |
|       | Average            | 0     | 62      | <b>2.3</b> | 49.8    | 3.9   | 30.3    | 3.6   | 23      | 5.2   | 18.2    |
| B     | Pipe 1             | 0     | 62      | 3          | 45      | 3.9   | 28      | 4.1   | 21.9    | 5.9   | 15      |
|       | Pipe 2             | 0     | 62      | 2.5        | 48      | 3.5   | 25.7    | 4.2   | 19.1    | 5.6   | 15.9    |
|       | Average            | 0     | 62      | <b>2.7</b> | 46.5    | 3.7   | 26.9    | 4.2   | 20.5    | 5.8   | 15.5    |

The width (mm) of the  $T_2^*$  drop is also cited. "A" stands for empty pipe (active) and "B" for iron filled pipe (baseline)

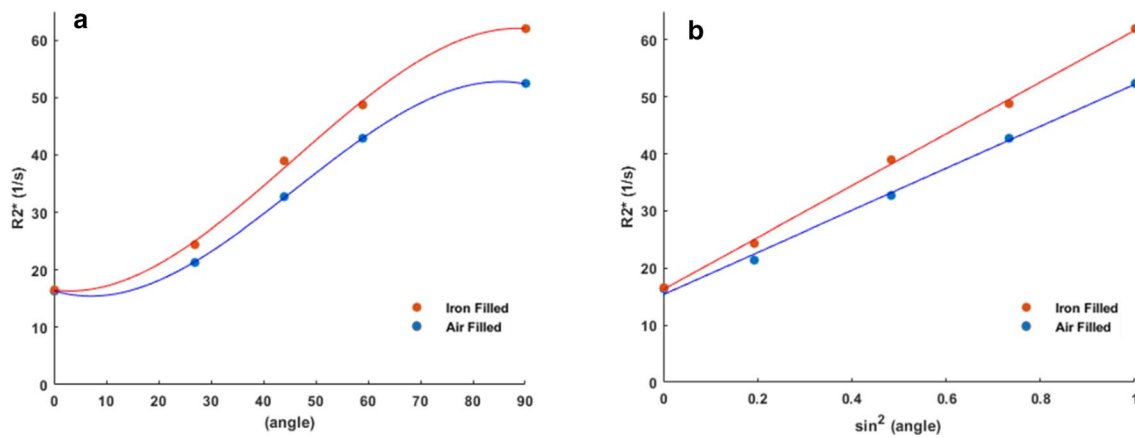


**Fig. 5** The  $R2^*$  (1/sec) over angle  $\theta$  (a) and over  $\sin^2\theta$  (b)

experiment was performed utilizing a GRE-EPI sequence with the parameters shown in Table 1. Each BOLD series consisted of 40 dynamic volumes, 20 for baseline state (state B) and 20 for active state (state A). The layout of the paradigm was 10B, 10A, 10B, 10A in this order.

The whole procedure was performed for the first two positions of the phantom. Regarding the first position, the pipes were parallel to  $B_0$  ( $\theta = 0^\circ$ ) and for the second position the angle was measured as  $\theta = 27^\circ$ . Concerning the first position ( $\theta = 0^\circ$ ) and according to the  $T2^*$  measurements (Table 2), no BOLD contrast was expected. Regarding the second position ( $\theta = 27^\circ$ ), the width of the signal drop for the corresponding  $T2^*$  measurements in Table 2 was 2.3 mm and 2.7 mm for the active and baseline states, respectively. Both values are less than 3 mm, which is the voxel size of the BOLD images. As a result, the active areas in the BOLD images should appear only in rows of just one or two pixels.

To further test the potential use of the phantom for BOLD optimization, the above BOLD series ( $\theta = 0^\circ$  and  $27^\circ$ ) were also obtained with various TEs. Percentage (%) signal difference and statistical  $t$  value tests were performed for evaluating the effect of TE parameter on the MoCo data.

### Post-processing of the BOLD images

Image processing (Mean active, Mean baseline, Numerical difference, percentage (%) difference) and statistical  $t$  value maps were constructed with the in-house software (QMRI utilities—X). For the calculation of the mean Active ( $\text{Mean}_{\text{active}}$ ) and mean Baseline ( $\text{Mean}_{\text{baseline}}$ ) maps, the mean value for each pixel was calculated as the average value from the 20 volumes for the active state and as the average value for the baseline state for the rest 20 volumes. The post-processing procedure was performed for both the raw acquisition (GRE-EPI scans) data and the motion correction (MoCo) data. The MoCo images were produced by the

vendor's software by applying motion correction algorithm on the EPI images.

Following that, the numerical difference:

$$\text{Diff} = \text{Mean}_{\text{active}} - \text{Mean}_{\text{baseline}} \quad (1)$$

and the corresponding percentage difference (%) were calculated on a pixel basis.

$$\text{Diff}(\%) = \frac{\text{Mean}_{\text{active}} - \text{Mean}_{\text{baseline}}}{\text{Mean}_{\text{baseline}}} \times 100 \quad (2)$$

Finally, the statistical  $t$  maps were produced utilizing the following equation [22]:

$$t = \text{Diff} \times \frac{\sqrt{N}}{Sd_{\text{active}} + Sd_{\text{baseline}}}, \quad (3)$$

where Diff is the numerical difference between mean active and mean baseline (1),  $Sd_{\text{active}}$  and  $Sd_{\text{baseline}}$  are the associated standard deviation of each state (A, B) per pixel and  $N = 40$  is the number of images.

### Phantom's stability

Five measurements of the BOLD signal were performed within a period of 1 month. The stability of the phantom was evaluated by calculating the coefficient of variation (% CV) in both states (A and B) according to the following equation:

$$\%CV = \frac{SD\text{Signal}(1, 2, 3, 4, 5)}{\text{meanSignal}(1, 2, 3, 4, 5)}. \quad (4)$$

The region of interest (ROI) was positioned on the pipes including 10 pixels, for the mean active map, the mean baseline map, the difference map and the  $t$  - value map accordingly.

## Results

### T2\* measurements

In Fig. 3, the T2\* parametric maps are shown at the five different positions ( $0^\circ$ ,  $27^\circ$ ,  $44^\circ$ ,  $59^\circ$ ,  $90^\circ$  as measured on the maps). The peak R2\* values over the angle  $\theta$  and over the  $\sin^2\theta$  are presented in Fig. 5 for both states, iron filled and empty pipe. The data of each state over the  $\sin^2\theta$  function are fitted with two straight lines:  $y_{\text{iron}} = 45.3689x + 16.2811$  and  $y_{\text{air}} = 36.8160x + 15.3827$ . The correlation coefficients of the fitting lines are  $r^2_{\text{iron}} = 0.9971$  and  $r^2_{\text{air}} = 0.9986$ , respectively.

### BOLD experiment

At position one ( $\theta = 0^\circ$ ) no BOLD contrast was achieved, as expected. T2\* measurements (Table 2) indicate that the change of the medium in the pipe has no impact to the T2\* of the area. The experiment was repeated choosing various TEs with the same result.

At position two ( $\theta = 27^\circ$ ) the BOLD contrast was apparent at the vendor's software for all the TE values. After the post-processing, the signal intensity over time was measured for both raw and MoCo data. The results are presented (Fig. 6).

The two states of the phantom produce an adequate signal change. A signal drop is observed during each baseline state (state B) and a signal rise is observed for each active state (state A). The statistical t maps in mosaic are presented (Fig. 7 a, b). The maps were constructed utilizing Eq. (3), where a strong correlation was observed between

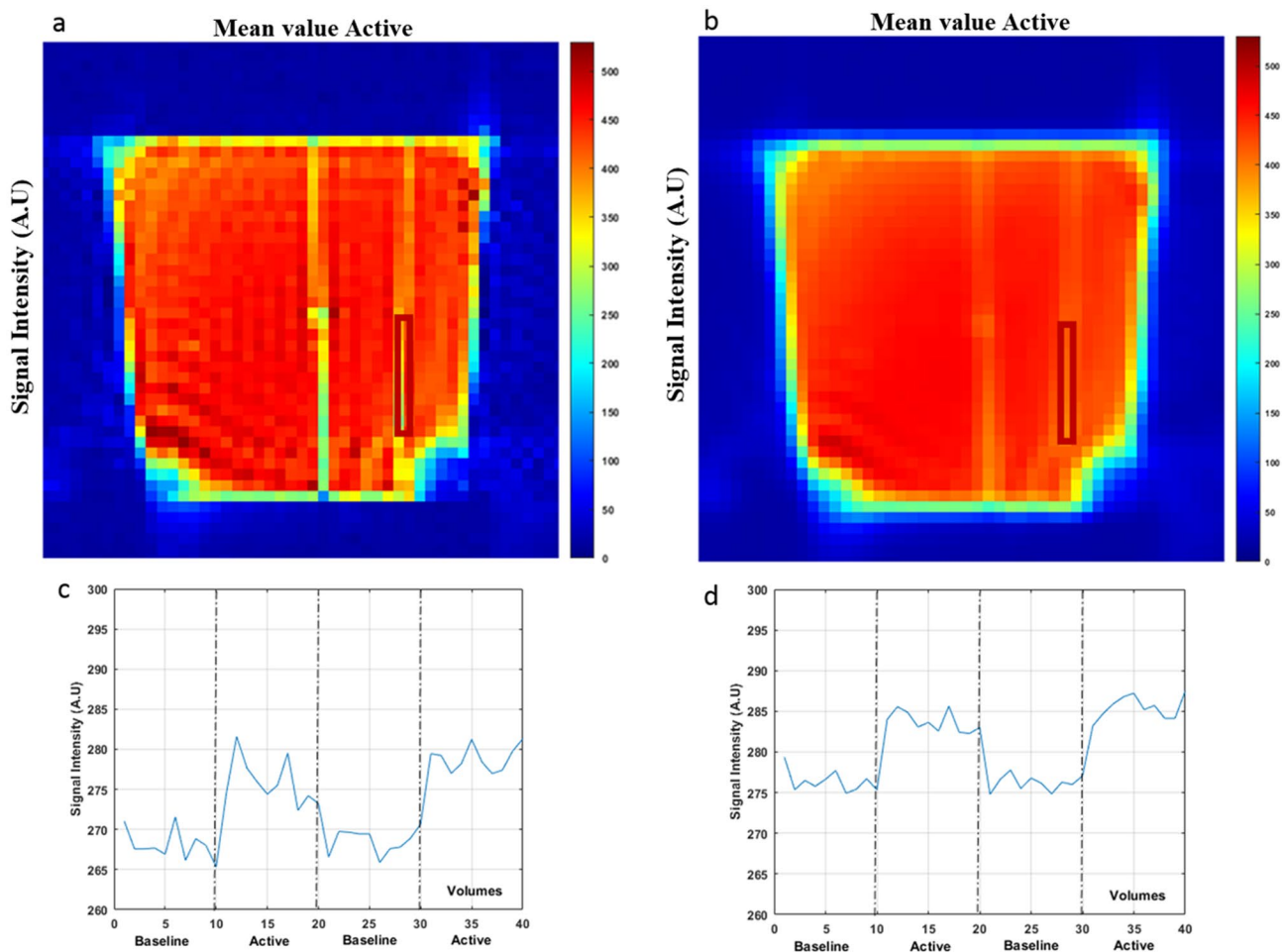


**Fig. 6** The mean active signal maps for both raw and MoCo data (a and b). The corresponding signal intensity over time is presented (c and d). The selected ROI is also shown

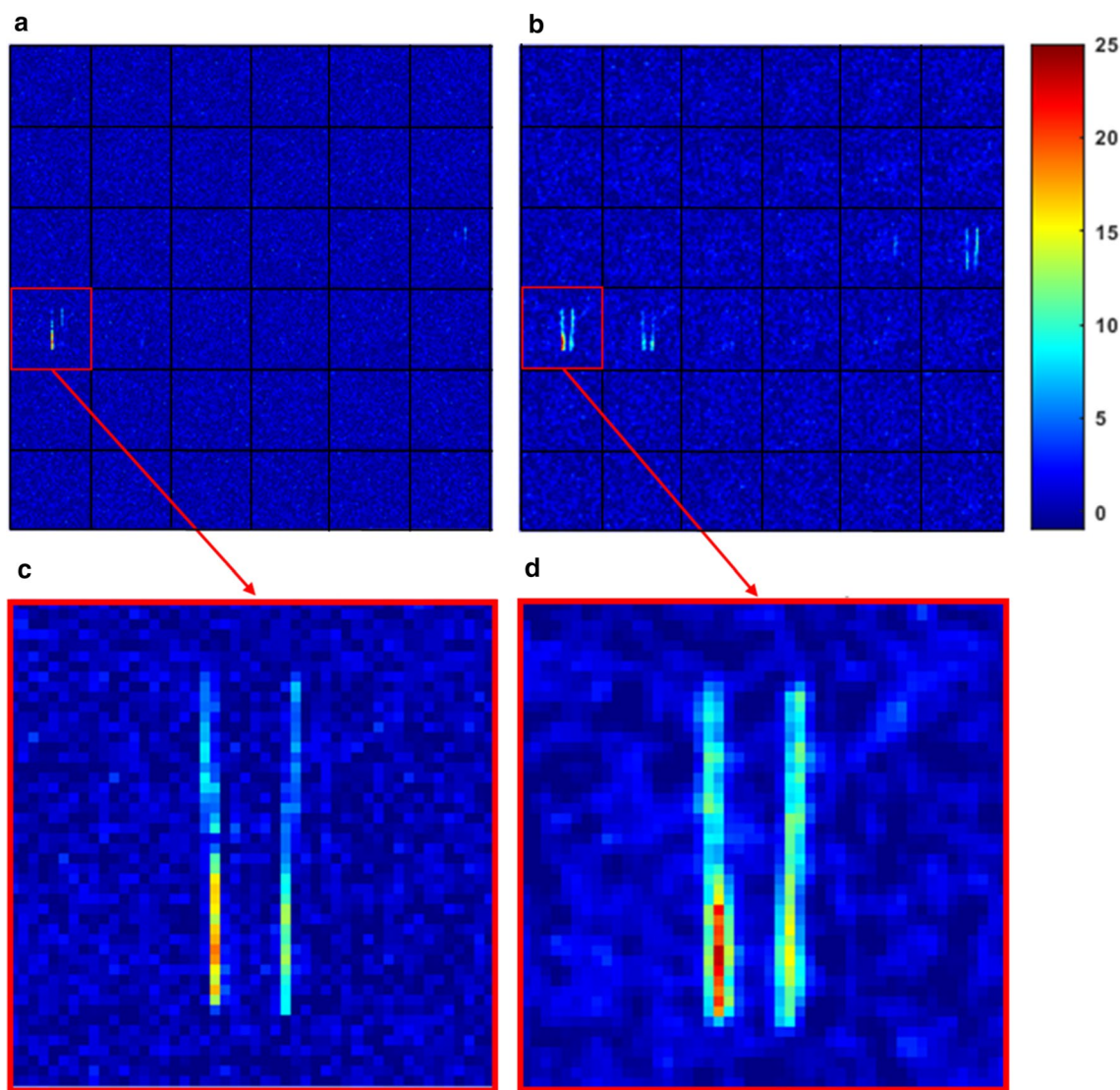


**Fig. 7** The statistical  $t$  maps for both raw (a) and MoCo data (b) in mosaic preview/format for all slices. The central slice of the activation area is presented enlarged (c and d)

the activation area and the  $t$  map value, by superimposing the two image datasets, and visually inspecting the fused images. No registration was required, since the two datasets are in the same coordinate system. The results are presented for both raw and MoCo data in mosaic preview/format. The enlarged statistical  $t$  value maps of the slices depicting the activation are also cited (Fig. 7c, d).

The relevant coefficients of variation—% CV for all five measurements are presented in Table 3.

The measured CV was lower than 2% for all measurements. This applies for measurements in the pipes' region but also in areas away from the pipes (non-pipe regions).

The (%) signal difference and the statistical  $t$  value over the different TEs are presented in Fig. 8. The peak of the curve is observed at approximately 60 ms TE.

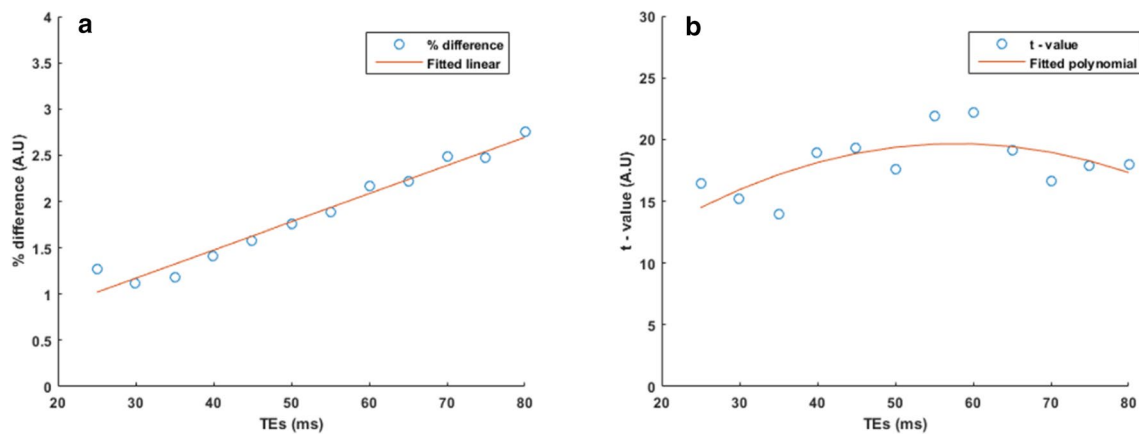
## Discussion

The important outcome of this study, presented in Fig. 5, is that the  $R2^*$  difference between the baseline and the active state (B–A state) depends on the angle  $\theta$ . Thus, the strength of the produced BOLD contrast can be adjusted by changing the angle  $\theta$ . The  $R2^*$  dependence on the angle  $\theta$  between the pipes and  $B_0$  disclosed a similar behavior to the approximation of  $\sin^2\theta$  as shown in previous studies [16–18]. The fitting correlation coefficients  $r^2_{\text{iron}} = 0.9971$  and  $r^2_{\text{air}} = 0.9986$  can be considered acceptable for this first approximation. The equation that describes this angular dependence has, also, other angular components [18], but  $\sin^2\theta$  seems to be the dominant component. To



**Table 3** The relevant coefficient of variations (% CV) over the five (5) measurements. The ROI was positioned in pipe region (upper) and non-pipe region (lower) for both raw and MoCo data

| Pipe region         | MoCo % CV | Raw % CV |
|---------------------|-----------|----------|
| Mean active         | 1.77      | 1.99     |
| Mean baseline       | 1.57      | 1.86     |
| Mean % difference   | 0.14      | 0.16     |
| <i>t</i> -value map | 0.28      | 0.35     |
| Non-pipe region     | MoCo % CV | Raw % CV |
| Mean active         | 1.37      | 1.46     |
| Mean baseline       | 1.44      | 1.5      |
| Mean % difference   | 0.05      | 0        |
| <i>t</i> value map  | 0.02      | 0.01     |

**Fig. 8** Signal (%) difference over TEs (a). *t* value statistical over TEs (b). The optimal fit of the data is included. The same ROI of Fig. 6 was selected

evaluate this angular dependence accurately, more detailed measurements and calculations should be performed.

Another parameter which can affect the strength of the produced BOLD contrast is the medium chosen to be injected in the pipe. In this preliminary study, air and iron solution were chosen to produce the active and baseline states, accordingly. Air and iron solution are both paramagnetic, but with a significant difference in susceptibility [23]. The solution concentration, which, also, affects the BOLD strength, can easily be modified. Other mediums to be injected could be considered for evaluation of their effect in future studies.

Phantom's operation was relatively easy by injecting the mediums to switch from each state to the other. As seen in Fig. 6, the switching between the two states was fast enough to provide a synchronized signal change with the BOLD acquisition. All the BOLD active images show a signal rise as compared to the baseline images acquired. This applies for both raw and MoCo images. MoCo according to vendor performs interpolation, reducing in this way, the relative

motion between the data sets. Moreover, MoCo algorithm affects the actual values of the pixel signal which in turn, affects the final results even if the phantom is not moving. In Fig. 6a, the activation areas in the raw images appear in well-located rows of one or two pixels in the phantom's imaging volume. This is in accordance with the T2\* measurements (Table 2; Figs. 4, 5). In the corresponding MoCo maps the same activation area appears in wider rows (Fig. 6b). So practically, as it can be seen in Fig. 7, MoCo results deteriorate the static spatial specificity as compared to the raw results. This observation highlights another advantage of the proposed method, through which the spatial specificity of BOLD sequences and algorithms can be examined: the presented dynamic phantom can produce an activation area consisting of only one pixel (when slices are perpendicular to the pipes). This can be a big advantage over the existing BOLD phantoms, which produce larger activation areas of several pixels.

The reproducibility of the phantom is acceptable. The measured CV according to Table 2 was lower than 2% in all

cases. The phantom can be considered reliable for repeatable recreations of BOLD contrast.

Although the BOLD volumes acquired (40) were fewer than those that are usually used clinically (at least 60), they were enough to produce an adequate statistical difference for the BOLD signal. Furthermore, investigation of other sequence parameters such as TE, which is an important parameter for the BOLD sensitivity, was also feasible.

As expected, the % signal difference increases in accordance with the TE, while the maximum  $t$  value was found to be at TE ~ 60 ms (Fig. 8). Both results are in agreement with previous experimental measurements [7]. Moreover, theoretical calculations have revealed that the maximum  $t$  value can be achieved using a TE equal to the measured  $T2^*$  of the medium [24], which in this case was situated in a range between 50 and 60 ms at the activation areas. The measured  $t$  values though, showed a deviation of the fitting curve because of the small statistical sample that was used.

Although, the measured  $T2^*$  (62 ms) of the 2% (w/v) agarose gel was comparable to the average  $T2^*$  of the gray matter (60–80 ms) measured at 1.5 T [11], the  $T2$  and  $T1$  values of the gel used in this study do not simulate the respective values of the gray matter. The  $T2$  and  $T1$  simulations were above the scope of this study and to keep the manufacturing procedure simple, a simple 2% (w/v) agarose gel was used.  $T1$  and  $T2$  values of the gel used were approximately 2100 ms and 70 ms, respectively. [13] Future work should, take under consideration other parameters such as the  $T1$  and  $T2$  values of the imaging medium and the configuration of the phantom. Physiological noise should also be simulated by an fMRI simulator, which is a critical parameter for the fMRI results. The size of the pipe could be even smaller to better simulate the size of a gray matter capillary, which has a diameter of a few micro meters and a wall thickness of approximately one micrometer. In our study, the diameter of the pipes used to simulate the vessels was larger (inner diameter 500 microns) and wall thickness of 175 microns. Also, more than one pipe could be used to better simulate the structure of the capillaries in brain tissue, where more ‘pipes’ (vessels) run through a single voxel in different orientations. Other limitations of this study, should be also noted. The pipelines used in this study were not absolutely straight. As a result, the relative position of the pipe in the voxel (Fig. 2) is not the same for all the voxels in the same slice. This is the reason behind the inhomogeneous signal course along the physical  $z$ -axis and as it can be seen in Figs. 6a,b and 7, the distribution of the activation area is present not only in the central slice but also in the adjacent slices too. Manually switching from baseline to active state, especially in prolonged experiments, could be tiring for the operator to synchronize with the scanner. An option to solve that issue can be the use of an automatic MR compatible injector, as the ones used in clinical practice for

contrast agents. Moreover, further work is needed to calibrate the adjustable parameters of this phantom to be used as a comprehensive End-to-End fMRI tool. More specifically, the relationship between the activation area and the angle used should be more accurately measured using more phantom placements in different angles. A theoretical calculation of this relationship should also be performed. Another adjustable parameter that should be examined is the medium injected in the pipes. A signal producing medium could be worth studying. Iron solutions of lower concentrations could be examined or even other paramagnetic solutions.

To sum up, in this study a new method for physical BOLD simulation was introduced based on a novel dynamic fMRI phantom construction. The phantom’s fundamental structure mimics blood vessels in human tissue. It provides an adjustable BOLD contrast without using electrical circuits. This fMRI simulator can be used to evaluate BOLD sensitivity and specificity.

**Acknowledgements** Part of this work was financially supported by a research project entitled: “Conversion and Calibration of Magnetic Resonance Imaging System (MRI) in a measuring system of hyperthermia applications, using magnetically labelled nanoparticles”, Acronym: MRI-TEMPERATURE, Operational Program: Competitiveness, Entrepreneurship and Innovation, EPANЕК 2014-2020, “Research Create and Innovate” (EYDE-ETAK Code: PSKE T1EAK-00149, OPS 5029590).

**Author contributions** TB: conceptualization, formal analysis, investigation, validation, writing—review & editing. GK: conceptualization, formal analysis, investigation, writing—review & editing. GG: writing—review & editing, AHK: writing—review & editing, supervision. EP: writing—review & editing, supervision. TGM: writing—review & editing, visualization, supervision.

## Declarations

**Conflict of interest** The authors declare no conflicts of interest.

**Ethical approval** Ethical approval is not applicable in this phantom study.

## References

- Ogawa S, Lee T-M, Nayak AS, Glynn P (1990) Oxygenation-sensitive contrast in magnetic resonance image of rodent brain at high magnetic fields. *Magn Reson Med* 14:68–78
- Ogawa S, Lee TM, Kay AR, Tank DW (1990) Brain magnetic resonance imaging with contrast dependent on blood oxygenation. *Proc Natl Acad Sci U S A* 87:9868–9872
- Pauling L, Coryell CD (1936) The magnetic properties and structure of hemoglobin, oxyhemoglobin and carbonmonoxyhemoglobin. *Proc Natl Acad Sci* 22:210–216
- Liau J, Liu TT (2009) Inter-subject variability in hypercapnic normalization of the BOLD fMRI response. *Neuroimage* 45:420–430
- Hennig J, Speck O, Koch MA, Weiller C (2003) Functional magnetic resonance imaging: a review of methodological aspects and clinical applications. *J Magn Reson Imaging* 18:1–15

6. Friedman L, Glover GH (2006) Report on a multicenter fMRI quality assurance protocol. *J Magn Reson Imaging* 23:827–839
7. Olsrud J, Nilsson A, Mannfolk P, Waites A, Ståhlberg F (2008) A two-compartment gel phantom for optimization and quality assurance in clinical BOLD fMRI. *Magn Reson Imaging* 26:279–286
8. Cheng H, Zhao Q, Duensing GR, Edelstein WA, Spencer D, Browne N, Saylor C, Limkeman M (2006) SmartPhantom - An fMRI simulator. *Magn Reson Imaging* 24:301–313
9. Renvall V, Joensuu R, Hari R (2006) Functional phantom for fMRI: A feasibility study. *Magn Reson Imaging* 24:315–320
10. Chen T, Zhao Y, Jia C, Yuan Z, Qiu J (2020) BOLD signal simulation and fMRI quality control base on an active phantom: a preliminary study. *Med Biol Eng Comput* 58:831–842
11. Peters AM, Brookes MJ, Hoogenraad FG, Gowland PA, Francis ST, Morris PG, Bowtell R (2007) T2\* measurements in human brain at 1.5, 3 and 7 T. *Magn Reson Imaging* 25:748–753
12. Laubach HJ, Jakob PM, Loevblad KO, Baird AE, Bovo MP, Edelman RR, Warach S (1998) A phantom for diffusion-weighted imaging of acute stroke. *J Magn Reson Imaging* 8:1349–1354
13. Boursianis T, Kalaitzakis G, Pappas E, Karantanas AH, Maris TG (2021) MRI diffusion phantoms: ADC and relaxometric measurement comparisons between polyacrylamide and agarose gels. *Eur J Radiol* 139:109696
14. Yablonskiy DA, Haacke EM (1994) Theory of NMR signal behavior in Inhomogeneous Tissues: The Static. *Magn Reson Med* 32:749–763
15. Yablonskiy DA, Reinius WR, Stark H, Haacke EM (1997) Quantitation of T2' anisotropic effects on magnetic resonance bone mineral density measurement. *Magn Reson Med* 37:214–221
16. Lee J, van Gelderen P, Kuo LW, Merkle H, Silva AC, Duyn JH (2011) T2\*-based fiber orientation mapping. *Neuroimage* 57:225–234
17. Bender B, Klose U (2010) The in vivo influence of white matter fiber orientation towards B0 on T2\* in the human brain. *NMR Biomed* 23:1071–1076
18. Oh SH, Kim YB, Cho ZH, Lee J (2013) Origin of B0 orientation dependent R2\* (=1/T2\*) in white matter. *Neuroimage* 73:71–79
19. Maris TG, Damilakis J, Sideri L, Deimling M, Papadokostakis G, Papakonstantinou O, Gourtsoyiannis N (2004) Assessment of the skeletal status by MR relaxometry techniques of the lumbar spine: Comparison with dual X-ray absorptiometry. *Eur J Radiol* 50:245–256
20. Maris TG, Papakonstantinou O, Chatzimanoli V, Papadakis A, Pagonidis K, Papanikolaou N, Karantanas A, Gourtsoyiannis N (2007) Myocardial and liver iron status using a fast T2\* quantitative MRI (T2\*qMRI) technique. *Magn Reson Med* 57:742–753
21. Kalaitzakis GI, Papadaki E, Kavroulakis E, Themistoklis B, Konstantinos Marias TGM (2019) Optimising T2 relaxation measurements on MS patients utilising a multi-component tissue mimicking phantom and different fitting algorithms in T2 calculations. *Hell J Radiol* 4:18–31
22. Parrish TB, Gitelman DR, LaBar KS, Mesulam MM (2000) Impact of signal-to-noise on functional MRI. *Magn Reson Med* 44:925–932
23. Schenck JF (1996) The role of magnetic susceptibility in magnetic resonance imaging: MRI magnetic compatibility of the first and second kinds. *Med Phys* 23:815–850
24. Posse S, Wiese S, Gembris D, Mathiak K, Kessler C, Grosse-Ruyken ML, Elghahwagi B, Richards T, Dager SR, Kiselev GV (1999) Enhancement of BOLD-contrast sensitivity by single-shot multi-echo functional MR imaging. *Magn Reson Med* 42:87–97

**Publisher's Note** Springer Nature remains neutral with regard to jurisdictional claims in published maps and institutional affiliations.